American Mineralogist, Volume 98, pages 1285–1296, 2013

Oxidation in CSPV experiments involving H_2O-bearing mafic magmas: Quantification and mitigation

THOMAS SHEA* AND JULIA E. HAMMER

Department of Geology and Geophysics, SOEST, University of Hawaii, Honolulu, Hawaii 96822, U.S.A.

ABSTRACT

A difficulty in performing high-temperature (>900 °C) experiments on near-liquidus hydrous mafic melts in gas-medium cold-seal pressure vessels (CSPV) is the tendency for H_2O in the fluid phase to dissociate and H_2 to diffuse through capsule material, leading to progressive oxidation of sample material. Negative consequences include premature stabilization of Fe-Ti oxide phases and commensurate deviation of the liquid line of descent toward silica enrichment. Moreover, time-variance of an intensive variable equal in importance to temperature or total pressure is an unwanted feature of any experimental study. Methodologies commonly employed to mitigate the oxidation problem, not without their own drawbacks, include incorporating CH_4 into the pressurizing gas, limiting run duration to 24 h, enclosing samples in Au-alloy capsules, and incorporating solid buffering assemblages to serve as indicators of f_{O_2} excursion. Using the Co-Pd-O system as a f_{O_2} sensor, we investigated progressive oxidation of basaltic andesite at 1010 °C and $P_{H_2O} = 150$ MPa. Our time-series of 12, 24, 36, 48, and 60 h run durations reveals that oxidation occurs at a very high rate (~3–4 log unit change in f_{O_2} in 48 h). Both the variability of f_{O_2} and magnitude of dehydration-oxidation are considered unacceptable for phase equilibria work. Incorporation of additional CH_4 serves only to offset the progressive oxidation trend toward a lower absolute range in f_{O_2}. Ultimately, rapid oxidation in CSPV hinders the chemical equilibration of experimental charges. To mitigate the issue, we propose the following solution: Incorporation of a substantial mass of Ni metal powder as an O_2 getter to the outer capsule successfully: (1) slows down oxidation; (2) stabilizes f_{O_2} at the nickel-nickel oxide (NNO) buffer after ~20 h; and (3) allows compositions to approach equilibrium. Runs much longer than 48 h may require one or more steps involving quenching and re-filling the pressure system with CH_4.

Keywords: Experimental petrology, oxygen fugacity, rates of oxidation, crystallization, chemical equilibrium

INTRODUCTION

Experimental petrology explores the effects of environmental conditions [e.g., temperature (*T*), pressure (*P*), time (*t*), oxygen fugacity (f_{O_2}), volatile content X_{fluid}, chemical composition X_{melt}] on the chemical behavior of magmas (e.g., Holloway and Wood 1988). Particularly pertinent to the field of volcanology are experiments that investigate the melting, crystallization, mixing, or vesiculation of magmas and the transport of chemical constituents (e.g., Kouchi and Sunagawa 1983; Blundy and Cashman 2008; Hammer 2008; Zhang and Cherniak 2010). Experiments using magmas of intermediate-to-felsic compositions at crustal pressures ($P > 1$ atm) and moderate temperatures ($T < 900$ °C) have increased in frequency in the past few decades (e.g., Hammer 2008 and references therein). Similar studies involving hotter ($T >$ 900–950 °C) hydrous mafic magmas at high pressures are sparse (e.g., Sisson and Grove 1993), mostly due to the technical challenges associated with volatile-rich melts at these temperatures. In many instances, high-*T* experiments involving mafic compositions are run using internally heated pressure vessels (IHPV; Holloway 1971; Muncill and Lasaga 1988; Moore et al. 1995; Moore and Carmichael 1998, Pichavant et al. 2002; Berndt et al. 2005; Di Carlo et al. 2006; Simakin et al. 2009), because they allow for large volumes of material and accommodate higher *P* and *T* conditions than cold-seal pressure vessels (CSPV; Holloway 1971). Despite their being used more often for colder, more silicic experiments (e.g., Hammer 2008 and references therein), CSPVs are increasingly used for hotter, hydrous experiments (e.g., Métrich and Rutherford 1998; Coombs et al. 2000; Hammer et al. 2002). IHPVs are relatively expensive, difficult to maintain and operate in comparison with CSPV apparatus (Lofgren 1987). Given the growing interest in explosive mafic volcanism (e.g., Houghton and Gonnerman 2008; Di Traglia et al. 2009), there is an opportunity for intensified use of CSPVs in laboratory experimentation involving hydrous mafic magmas. Thus, it is important to evaluate the practical limits of methods already in common use to impose and maintain desired thermodynamic conditions.

Oxygen fugacity (f_{O_2}), along with *P* and *T*, is widely recognized as an important factor controlling magmatic crystallization sequences and liquid lines of descent (e.g., Muan 1958; Osborn 1959; Sisson and Grove 1993; Toplis and Carroll 1995; Berndt et al. 2005; Hammer 2006; Feig et al. 2010). Oxygen fugacity exerts a direct control on the valence state of metal elements (dominantly Fe^{2+}/Fe^{3+} in natural magmas), which, in addition to controlling the appearance of iron-bearing oxides (Carmichael and Nicholls 1967; Toplis and Carroll 1995), dictates how Fe partitions into

---

* E-mail: tshea@hawaii.edu

0003-004X/13/0007–1285$05.00/DOI: http://dx.doi.org/10.2138/am.2013.4253

iron-rich mafic phases such as olivine, pyroxene, and amphibole (Carmichael and Ghiorso 1990; Carmichael 1991; McCanta et al. 2004). Hence, f_{O_2} not only affects the presence of certain phases, but their composition (e.g., Mysen 2006) and formation temperatures as well. Because f_{O_2} can vary by 8–9 orders of magnitude in natural magmas (Carmichael and Ghiorso 1990), it is crucial for experimental apparatus to impose fugacity conditions that are appropriate for a particular natural setting.

In 1 atm, high-*T* experiments, f_{O_2} is regulated using variable proportions of gas mixtures (e.g., H_2 and CO_2) that react to produce small amounts of free oxygen (Nafziger 1971; Huebner 1987). This setup allows precise control over ambient f_{O_2} and facilitates examination of the behavior of volatile-poor magmas at planetary surface conditions. In stark contrast, controlling fugacity conditions in high-pressure hydrous experiments to study magmatic processes within the crust is more challenging due to the tendency of dissolved H_2O to dissociate. Hydrogen diffuses through capsule walls, causing the partial pressure of oxygen to progressively increase during the course of the experiment.

Relatively low-*T* (i.e., <900–950 °C) hydrous experiments are typically carried out in vessels made of Co- or Ni-rich alloys (e.g., "Stellite-25," "Waspaloy") that use a supercritical fluid (H_2O) as a pressurizing medium (Edgar 1973). These alloys intrinsically impose an f_{O_2} on enclosed samples that is close to the Co-CoO or Ni-NiO oxygen buffers (Gardner et al. 1995). In contrast, higher temperature (>900–950 °C) runs entail the use of stronger materials (e.g., molybdenum-based alloys with Ti and Zr; TZM). In such experimental setups, controlling and monitoring f_{O_2} is problematic because the pressurizing medium is not H_2O. The lack of such a hydrogen buffer can thus lead to strong H_2 gradients across the experimental capsule wall (Scaillet et al. 1992).

After a brief summary of available methods to control and monitor oxygen fugacity conditions, we test the degree to which f_{O_2} varies throughout experiments at high temperatures (>950 °C) and pressures (>100 MPa) involving mafic (basaltic-andesite) magma. We examine the time-variance of f_{O_2} and thereby the rates of oxidation in CSPV experimental setups. We find that oxidation progresses very rapidly, and prevents the samples from reaching chemical equilibrium. We provide detailed guidelines for preventing rapid increases in f_{O_2} that involve introducing CH_4 into the pressurizing gas and employing a simplified solid-medium oxygen buffering technique. It is hoped that these provisions will benefit laboratory investigations involving hydrous mafic magmas.

BACKGROUND

Controlling f_{O_2} at high *P* and *T*

Several approaches have been developed to impose a desired f_{O_2} in experimental runs in high-*P* studies (cf. Table 1 for methods adopted in hydrous mafic magma studies using CSPV). The first and simplest procedure involves the introduction of a small amount of hydrogen-containing gas (H_2 or CH_4) into the vessel prior to full pressurization with Ar gas. The CH_4 dissociates at experimental temperature to make H_2, thus reducing the gradient in hydrogen across the capsule wall (e.g., Gaetani et al. 1994). We demonstrate below that the increased f_{H_2} outside the sample capsule shifts the sample f_{O_2} to more reduced conditions beginning shortly after the vessel is inserted into the high-*T* furnace. While this procedure allows setting the initial fugacity conditions to a given value, H_2 continuously diffuses out of the capsule and vessel, thus driving the system to progressively more oxidized conditions (Scaillet et al. 1992). The "Shaw-membrane" technique is based on the same principle, the major improvement being that a regulated feed of H_2 gas through a permeable membrane maintains nearly constant f_{H_2} and f_{O_2} fugacity conditions (Shaw 1963). Hewitt (1978) and later Scaillet et al. (1992) and Schmidt et al. (1995) successfully applied this technique in CSPV; briefly, an H_2-permeable membrane made of Pt or AgPd and mechanically supported by an inert filling (e.g., quartz or alumina grains, to avoid rupture during pressurization) is connected to a hydrogen source and transducer system located outside the vessel by a stainless steel capillary. This technique is, however, not as popular since it requires non-negligible physical modifications to the experimental apparatus (e.g., Gunter et al. 1987; Scaillet et al. 1992) and requires the use of larger volumes of an explosive gas. Another approach was devised by Eugster (1957), and involves the use of solid oxygen buffers such as Ni-NiO (NNO), Co-CoO (CCO), or fayalite-magnetite-quartz (FMQ) inside the noble metal sample capsule that react to maintain f_{O_2} at a constant value until the buffer is exhausted (Huebner 1971). The solid buffers are usually placed inside sealed capsules along with the starting material, and the various reactions are initiated, capturing or releasing O_2, if the ambient oxygen fugacity varies from the f_{O_2} value of the corresponding buffer. The main drawback of

TABLE 1. Abridged list of hydrous experiments involving mafic magmas at high temperatures (i.e., having at least some runs with $T \geq 950$ °C) carried out in cold-seal pressure vessels, and the techniques employed to control and monitor oxygen fugacity

Study	Starting composition	Setup	*T* (°C)*	*P* (MPa)†	*t* (h)‡	f_{O_2} control§	f_{O_2} sensing‖
Gaetani et al. (1994)	Basaltic-andesite	CSPV	1005–1100	200	3–24	GP(Ar-CH_4), SB	–
Parman et al. (1997)	Komatiite	CSPV	1026–1257	100–200	5–41	GP(Ar-CH_4), SB	–
Grove et al. (1997)	Andesite	CSPV	865–1050	100–200	18–66	I, SB	–
Metrich and Rutherford (1998)	Basaltic-hawaiite	CSPV	1009–1135	27–80	8–38	GP(Ar-CH_4), SB	–
Dann et al. (2001)	Fe-basalt	CSPV	960–1105	100–200	9–49	GP(Ar-CH_4), SB	–
Hammer et al. (2002)	Andesite	CSPV	850–1050	50–225	22–96	GP(Ar-CH_4), SB	–
Szramek et al. (2006)	Basaltic-andesite	CSPV	940–1075	50–200	8–30	GP(Ar-CH_4), SB	–
Barr et al. (2009)	Komatiite	CSPV	1125–1275	180–210	3–7	GP(Ar-CH_4), SB	–
This study	Basaltic-andesite	CSPV	1010	150	6–60	GP(Ar-CH_4), SB	Co-Pd MS

Notes: CSPV = Cold-seal pressure vessel. GP = Gas pressure control of f_{O_2} by varying gas proportions. MS = Double capsule metal-metal oxide sensor technique (Taylor et al. 1992). I = f_{O_2} intrinsically controlled by vessel alloy. SB = Solid buffer technique (see Eugster 1957; Huebner 1971).

* Range of experimental temperatures investigated.

† Range of experimental pressures.

‡ Range of experimental durations.

§ Method(s) utilized to impose oxygen fugacity.

‖ Method(s) utilized to measure oxygen fugacity.

oxygen buffers is that they are consumed rapidly, particularly at high *T* where hydrogen diffuses out of the experimental capsules more rapidly, and oxidation reactions are faster (e.g., Scaillet et al. 1992). Matthews et al. (2003) take advantage of the intrinsic buffering redox reactions that occur within alloys dominated by one of various metals (Ni, Co, W, Ti, Fe, and C) placed outside sample capsules, usually as filler rods. Wilke and Behrens (1999) use a boron nitride (BN) jacket that acts to slow down the loss of H through capsule walls. Both of these methods have only been tested at temperatures near the solidus of intermediate to mafic magmas (T = 750–850 °C).

Monitoring f_{O_2} conditions at high *P* and *T*

Oxygen fugacity can be monitored directly and in real-time using derivatives of the Shaw-membrane technique described above (e.g., Scaillet et al. 1992) or indirectly using fluid or solid sensors. The Ag-AgCl-HCl fluid f_{H_2} sensor technique takes advantage of H diffusion through the enclosing capsules and the ensuing Ag/AgCl ratio variation changing the pH of the solution, which is measured after quenching (Frantz and Eugster 1973). Taylor et al. (1992) noted that several problems such as fluid evaporation and dilution effects strongly influence the calculation of f_{O_2}, and that the range of applicability of this technique is uncertain above T = 800 °C. Taylor et al. (1992) thus recommended the use of solid redox sensors instead. The latter exploit the capacity of metal-metal oxide systems (e.g., CCO, NNO), alloyed with pure metals (e.g., Pd, Pt), to compositionally self-adjust to changes in f_{O_2}. In this fashion, fugacity conditions can be retrieved by analyzing the resulting alloy composition and computing ambient f_{O_2} through a series of calibration equations (O'Neill and Pownceby 1993; Pownceby and O'Neill 1994). The solid sensor method is preferred since it is readily applicable and requires no mechanical modification to the CSPV setup.

EXPERIMENTAL METHODS

This section describes the experimental setup used for this investigation. Figure 1a illustrates schematically the various elements that enter our CSPV design along with the main reactions that occur during experimental runs.

Starting material

A natural sample of basaltic-andesite (bulk composition ~55 wt% SiO_2, ~5% Na_2O+K_2O, Table 1) lava from Mascota volcanic field (Mexico), characterized in previous petrological and phase equilibria studies (Lange and Carmichael 1990; Moore and Carmichael 1998), was used as starting material (sample Mas22). The lava is glass-poor (72 vol% groundmass microlites) and encloses phenocrysts of olivine, plagioclase, and clinopyroxene. Centimeter-sized subsamples of this lava were crushed coarsely (tens of micrometers to millimeter-sized particles) to avoid contamination by possibly zoned phenocryst cores. This ensures that only the "reactive" magma participates in the chemical budget of the system, implying that equilibrium should only be partial (i.e., the melt, the newly formed phases, and phenocryst rims) (Pichavant et al. 2007). About 0.1–0.2 g of starting material was placed into a 5 mm OD $Ag_{70}Pd_{30}$ capsule along with enough water to ensure saturation of an H_2O-rich fluid phase upon pressurization (see below). An important assumption (discussed further below) is that Fe was not significantly removed from the melt by reaction with the surrounding AgPd capsule walls.

Experimental procedures

All experimental charges consisted of the crushed starting material and a CoPd sensor capsule (see below for description of the sensor). In some experiments,

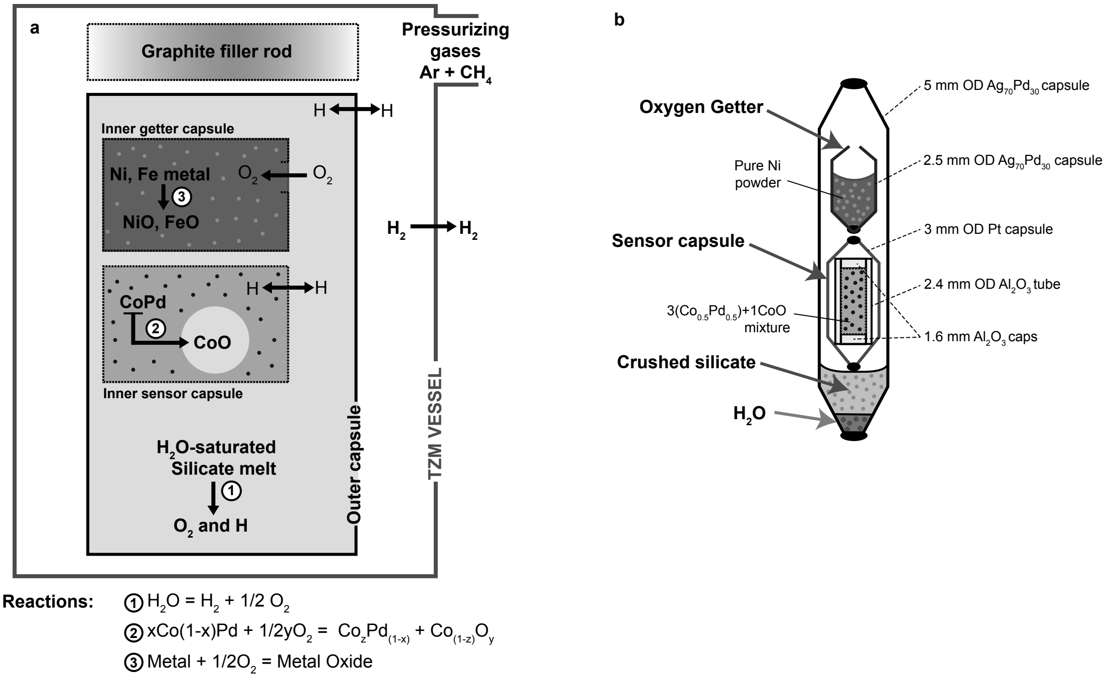

FIGURE 1. (**a**) Simplified box-sketch of the various components and reactions that are found in the CSPV experiments described herein. The largest bounding box represents the cold-seal TZM pressure vessel, which is pressurized using a mixture of argon and methane. The outer capsule containing the experimental charge is welded, and only hydrogen can diffuse in or out. (**b**) Specific setup used for experimental charges. The crushed starting material is placed at the bottom along with enough H_2O to saturate the melt. The CoPd sensor capsule and the Ni or Fe oxygen getter are inserted on top, with the getter being only welded shut at the bottom to allow oxygen to circulate and react with the Ni or Fe. The sensor capsule is welded shut on both ends to only let hydrogen diffuse in and out.

pure Fe or Ni oxygen getters (Fe- or Ni-OG, see below) were inserted above the sensor to test whether the getters succeeded in maintaining fugacity conditions at steady values. All runs presented here were conducted in the same TZM cold-seal pressure vessel for consistency. Two experiments were also carried out using a molybdenum-halfnium-carbide (MHC) vessel and showed indistinguishable results; another set of experiments were carried out at higher *T* (1050 and 1075 °C) to test whether the OG was equally effective at conditions favoring faster reaction rates; these sets of experiments are not detailed herein. For all the experiments presented in this paper, conditions of pressure of 150 MPa and a temperature of 1010 °C were chosen based on the phase diagram of Moore and Carmichael (1998) to produce a phase assemblage that includes liquid, plagioclase, clinopyroxene, and olivine. About 8–10 wt% H_2O was initially added to the experimental charge to ensure vapor saturation (~4.5 wt% at 150 MPa, based on solubility calculated from Moore et al. 1998). Once the capsule was welded shut and placed at the bottom of the vessel, a graphite filler-rod was inserted that serves two purposes: (1) it ensures that there is no space available for convection within the vessel, which could potentially influence the internal temperature (Boettcher and Kerrick 1971); and (2) it helps maintain reducing redox conditions inside the vessel during the experiment (e.g., Huebner 1971; Matthews et al. 2003). It is worth noting that, over time, using filler-rods with compositions different from the vessel may potentially change the structure and thereby the strength of the alloy vessel. Yet an additional worry with metallic filler-rods (Fe, Ni, Co, Ti, and W) is the possibility of sintering with the vessel if not properly isolated by Pt spacers (Matthews et al. 2003).

The temperature of the furnace outside the pressure vessel is accurately controlled by a B-type thermocouple (TC). Because CSPVs do not readily allow for direct measurements of *T* during high-*P* runs through additional internal TCs, the temperature requires an indirect calibration (Boettcher and Kerrick 1971); first, the CSPV setup is introduced in the furnace at 1 atm mounted with a K-type TC welded to a coned closure piece. The temperature measured by the K-type TC inside the vessel is thereafter considered to be representative of the sample temperature. Considering that the TC used for calibration has a sensitivity of about ±2 °C and that smaller *T*-variations may occur during the run, we estimate that temperature was constant within ±5 °C.

Total pressure ($P_{TOT} = P_{CH_4} + P_{Ar}$) was directly monitored within the pressurized line with a high precision (±0.007 MPa) Honeywell Sensotec transducer checked against a factory-calibrated 500 MPa Heise bourdon tube fluid gauge for accuracy. After introduction of CH_4 and Ar gases, pressure was rapidly brought to the desired run pressure and the vessel inserted into the furnace. Upon completion of the experiment, the vessel was extracted and forced-air cooled for 5–10 s and then plunged into water. The time to reach the glass transition is estimated to be <15 s. This cooling procedure resulted in the formation of quench crystals (≤10 μm) in some experiments.

f_{O_2} sensors: The CoPd-CoO system

Oxygen fugacity was monitored using solid binary alloy sensors (Taylor et al. 1992). The Co-CoO system was preferred over the Ni-NiO system because it spans a wider range of fugacities (~NNO–1.5 to NNO+5). A 50–50 mol% mixture of powdered reagents of Co and Pd (>99.99% purity) were finely ground in acetone, inside an agate mortar, until a fine, homogeneous material was obtained. The resulting CoPd powder was dried and further mixed with ground CoO grains in the molar ratio 3 parts metal/1 part metal oxide. This final CoPd-CoO mixture was then inserted into a 15 mm length, 2.4 mm OD, 1.6 mm ID porous alumina tube capped by a cemented alumina plug 1.6 mm in diameter and 1 mm in length, and gently compacted into a pellet. The alumina tube was then capped, cemented, and inserted into a 3 mm OD Pt capsule. The capsule was welded shut and placed inside the larger capsule containing the starting material (Fig. 1). To test whether the presence of H_2O within the sensor capsule affects the CoPd alloy formation and thus the recorded f_{O_2}, one experiment was performed with H_2O added. The f_{O_2} calculated from both H_2O-rich and H_2O-poor sensors was indistinguishable (cf. Table 2); as a result, the rest of the sensors were welded shut with no additional water. Because the CoO-CoPd sensor technique was developed at 1 atm (Taylor et al. 1992), we also tested whether pressure could affect the f_{O_2} calculated from the sensor compositions; a lower temperature (880 °C) experiment was carried out using a horizontal "clamshell" furnace and a Rene-style waspalloy CPSV pressurized at 200 MPa by water, and using a Ni rod to buffer oxygen fugacity around NNO. The resulting sensor yielded a nearly perfect f_{O_2} of NNO+0.05, suggesting that pressure has little or no influence on the CoO-CoPd system compared to temperature.

f_{O_2} buffers: Oxygen getters

Because f_{O_2} is expected to increase in the sample capsule during the experiments by dissociation of H_2O and diffusive loss of H_2 through the vessel, simple metal oxygen getters (OG) were used in some experiments to test whether f_{O_2} could be maintained at buffer values for longer periods. These OGs serve the same purpose as typical double buffer capsules used in other experiments (e.g., Huebner 1971) but initially contain no metal oxide. Two OGs consisting of high-purity (i.e., >99.99%) Fe and Ni reagents were tested. Since intrinsic f_{O_2} of the sample is well above the iron-wüstite buffer curve, Fe reacts with the environment and captures O_2 to form FeO as soon as the experiment is initiated. In the second case, oxidation of Ni begins when f_{O_2} reaches the NNO buffer. The powder of pure metal is inserted into 2.5 mm OD $Ag_{70}Pd_{30}$ tube with only the bottom crimped and welded (Fig. 1b). If all the available Fe or Ni is exhausted through oxidation, f_{O_2} is no longer maintained near the buffer values, and is expected to increase.

Variables tested: P_{CH_4}, *t*, and OG

A series of experiments were carried out with variable P_{CH_4} (0.3, 0.9, and 1.5 MPa) to evaluate the influence of initial CH_4 on the f_{O_2} inside the sample capsule. Next, P_{CH_4} was fixed at 0.3 MPa, and time-series runs of 6, 12, 24, 36, 48, and 60 h were conducted with no OG. In two separate 48 h experiments, CH_4 was replenished at *t* = 24 h without quenching the charge (i.e., by opening the vessel valve to a pressure line filled with either 0.3 or 5 MPa CH_4 and the balance Ar) to examine whether fugacity would remain at more reducing conditions. This procedure is hereafter referred to as "hot-swapping." Another longer run (72 h) was performed in a similar fashion but with quenching steps at *t* = 24 h and *t* = 48 h, during which the Ar+CH_4 mixture was purged and replenished with initial values. This practice is hereon referred to as "cold-swapping." To test whether OGs help maintain fugacity conditions constant, four additional experiments (two at *t* = 48 h and two at 60 h) using Fe or Ni were conducted. Finally, extra H_2O was added to one sensor capsule with the CoPd-CoO mixture, to check whether the water content influenced the evolution of f_{O_2}.

Analytical techniques

Glass chips, as well as solid cylindrical-shaped sensor rods retrieved from their capsules after quenching were mounted in epoxy for electron microprobe analysis (EMPA). Wavelength-dispersive spectrometry (WDS) analyses of glasses and metal alloys were performed with a JEOL Hyperprobe JXA-8500F at the University of Hawaii. A 15 keV acceleration voltage, 10 nA sample current, and a defocused 10 μm beam diameter were used for glass analyses. Counting times were: 10 s (Na), 20 s (Si, Al, Ca), 30 s (Fe, Mg, Ti), 40 s (Mn, P), and 50 s (K). Basaltic glass standards VG-2 and A99 (Jarosewich et al. 1980) were repeatedly measured to monitor analytic drift. For the analysis of CoPd alloy compositions, conditions were 20 keV, 30 nA, 5 μm beam diameter, and 30 s counting time. High-purity (>99.99 wt%) Co and Pd metal wires were used for standard calibration. Alloy compositions were also measured with energy-dispersive spectrometry (EDS) to compare with WDS analyses.

Experimental phase abundances could not be robustly obtained through mass balance between glass and mineral compositions due to the textural and chemical complexity of the run products (e.g., olivine destabilization in some runs, and pervasive zoning of olivine and clinopyroxene). Instead, phase abundances were determined using backscattered electron (BSE) images. Phases such as olivine, clinopyroxene, and oxides were easily distinguished from the glass by applying grayscale thresholds. In contrast, plagioclase crystals were outlined by hand in most cases. Because the starting material consists of crushed glass and crystals, fragments or entire phenocrysts from each phase are usually still present after terminating the experiments. Typically, the phases that crystallize during the run are either small individuals within the glass or rims around pre-existing large crystals. In most cases, the newly grown rims show slightly different contrasts within BSE images, allowing discrimination between pre-existing crystalline material from that which formed during the run. It is worth emphasizing that our phase abundance measurements are meaningful only in the context of experiments approaching a state of "partial" equilibrium (melt with newly formed crystals and phenocryst rims), but not in the context of "total" equilibrium (the whole system including phenocryst cores) (Pichavant et al. 2007).

RESULTS AND INTERPRETATIONS

Lack of Fe exchange between melt and experimental capsule

Various studies have reported that Fe from the melt can be lost to the capsule walls (e.g., Grove 1981; Gaetani and Grove 1998; Di Carlo et al. 2006; Barr and Grove 2010), while others described little to no Fe exchange in their experiments (e.g.,

TABLE 2. List of experiments with measured f_{O_2} and phase abundances; all experiments were run at T = 1010 °C and P_{total} = 150 MPa

Experiment	t (h)	P_{CH_4} (MPa)	OG*	X_{Co} (WDS)†	X_{Co} (EDS)‡	log f_{O_2}§	ΔNNO‖	ϕ_{Ol}#	ϕ_{Cpx}#	ϕ_{Pl}#	ϕ_{Mt}#	ϕ_{Gl}#
MAS_fO2_1	24	0.3	–	0.304(2)	0.293(6)	−10.28	−0.10					
MAS_fO2_1b	24	0.3	–		0.285(7)	−10.15	+0.03	0.036	0.019	0.245	0.008	0.692
MAS_fO2_2	24	1.5	–	0.517(6)	0.514(7)	−11.18	−1.00					
MAS_fO2_3	24	0.9	–	0.324(13)	0.338(10)	−10.48	−0.31					
MAS_fO2_4	48	0.3	–		0.132(7)	−8.66	+1.51	0.039	0.026	0.246	0.014	0.675
MAS_fO2_5	12	0.3	–		0.354(9)	−10.57	−0.39	0.022	0.028	0.163	0	0.786
MAS_fO2_6	36	0.3	–		0.164(12)	−9.06	+1.11	0.036	0.023	0.224	0.012	0.704
MAS_fO2_7	6	0.3	–		0.563(9)	−11.29	−1.11	0.021	0.022	0.112	0	0.845
MAS_fO2_8	24 × 2**	0.3 × 2**	–		0.902(7)	−8.02	+2.16					
MAS_fO2_9	24 × 3††	0.3 × 3††	–		0.514(7)	−11.18	−1.00					
MAS_fO2_10	48	0.3	Fe		0.208(17)	−9.52	+0.66					
MAS_fO2_13	48	0.3	Ni		0.268(4)	−10.03	+0.15					
MAS_fO2_15	60	0.3	Ni		0.130(7)	−8.64	+1.54	0.026	0.021	0.221	0.072	0.725
MAS_fO2_16	60	0.3	–		0.061(5)	−7.44	+2.74	0.007	0.026	0.211	0.025	0.730
MAS_fO2_17	48‡‡	0.3, 5‡‡	–		0.202(3)	−9.46	+0.72					
MAS_fO2_18	48§§	0.3§§	–		0.145(2)	−8.83	+1.34					

* Presence and type of oxygen getter.
† Composition of CoPd alloy analyzed using EMPA (1 standard deviation in parentheses, numbers correspond to last digits).
‡ Composition of CoPd alloy analyzed using SEM (1 standard deviation in parentheses, numbers correspond to last digits).
§ Log of oxygen fugacity calculated using the CoPd composition (see text).
‖ Departure of log f_{O_2} from the nickel-nickel-oxide buffer reaction.
\# ϕ = phase abundance as fraction of total, with Ol = olivine, Cpx = clinopyroxene, Pl = plagioclase, Mt = magnetite, Gl = glass.
** Experiment started with 0.3 MPa CH_4 replenished without quenching at t = 24 h.
†† Experiment that has been quenched and for which the initial CH_4 was replenished.
‡‡ Experiment started with 0.3 MPa CH_4, and replenished with 5 MPa CH_4 with no quenching step at t = 24 h.
§§ Experiment similar to MAS_fO2_4 but with extra H_2O added to the sensor capsule.

Spulber and Rutherford 1983; Sisson and Grove 1993; Grove et al. 1997; Parman et al. 1997; Barclay and Carmichael 2004). A potential consequence of Fe loss is the oxidation of the melt via the reaction $Fe^{o}_{melt} \leftrightarrow Fe^{o}_{alloy} + ½O_2$. To evaluate this possibility, EDS X-ray maps and profiles were performed on a polished capsule from an experiment run for >48 h. Although EDS cannot give the same accuracy and precision as EMPA (the detection limit of EDS is 0.2–0.3 wt% for most elements), for simple binary or ternary systems (i.e., AgPd ±Fe) we found that there was little difference between the two techniques (cf. CoPd analyses in next section). Neither the map nor the profiles revealed the presence of Fe in the capsule material, suggesting that Fe exchange was not significant. In addition, EMPA spots within the rims of experimental glasses, close to the contact between glass and capsule, are indistinguishable from those located in the middle of the glass chip. Thus, it is unlikely that Fe loss to the enclosing capsules was an important factor in the evolution of melt chemistry and thereby f_{O_2} during the experiments.

CoPd-CoO sensors

All retrieved sensor cylinders were about 5 mm in length and about 1–1.5 mm in diameter and were coated with a very thin discontinuous bright blue powder. This powder was analyzed and identified as Co-spinel ($CoAl_2O_4$), which likely formed as a result of a reaction between the alumina tubing (Al_2O_3) and the CoO. We consider this reaction to be inconsequential to the formation of the alloy for two reasons; first, the reaction is only very localized on the sensor surface. No Co-spinel is detected in the sensor interior. Second, the removal of some CoO does not affect the capacity of Co and Pd to alloy as fugacity changes (CoO is merely the product of the redox reaction).

In BSE images, sensors appear as mixtures of various proportions of grains (CoO) and interconnected blebs of metal (CoPd alloy) (Figs. 2a–2d). Chemical analyses revealed very little spatial variation throughout the sensors (i.e., typically <2 wt% variation in the alloy composition, Table 2). In one case where the experimental charge had been clearly corrupted (water was lost from a fissured capsule), the sensor contained large chemical variations (up to 30 wt% changes in Co within the alloy).

After analyses of the alloys were obtained, the proportion of Co was converted to f_{O_2} using an equation obtained through a combination of formulations by Taylor et al. (1992) and O'Neill and Pownceby (1993)

$$\log f_{O_2} = -2\log X_{Co} - \left(\frac{1}{2.3025RT}\right) \left\langle \begin{array}{l} \left(492186 - 509.322T + 53.284T\log T - 0.02518T^2\right) \\ + \left\{2\left(1 - X_{Co}\right)^2\left[-9.76T + 16445\left(4X_{Co} - 1\right)\right]\right\} \end{array} \right\rangle \quad (1)$$

where X_{Co} is the atomic fraction of Co in the CoPd alloy, T is temperature in Kelvin, and R = 8.3145 J/(mol·K) is the universal gas constant. Note that the pressure term is absent from this equation since it is inferred to have a negligible effect on the adjusting properties of such metal alloys at crustal-like pressures (Pownceby and O'Neill 1994). To facilitate the use of Equation 1, a calculation spreadsheet is provided in the supplementary material[1] for both Co and Ni-based sensors.

Repeat experiments of duration t = 24 h (same P, T, and amount of CH_4 gas in the initial pressurization step) show that the sensors behave very consistently, only showing ~0.03 variation in X_{Co}, which translates into oxygen fugacity uncertainties of about 0.5–0.75 log units. Analyses performed on the same sensors us-

---

[1] Deposit item AM-13-701, Deposit data table. Deposit items are available two ways: For a paper copy contact the Business Office of the Mineralogical Society of America (see inside front cover of recent issue) for price information. For an electronic copy visit the MSA web site at http://www.minsocam.org, go to the American Mineralogist Contents, find the table of contents for the specific volume/issue wanted, and then click on the deposit link there.

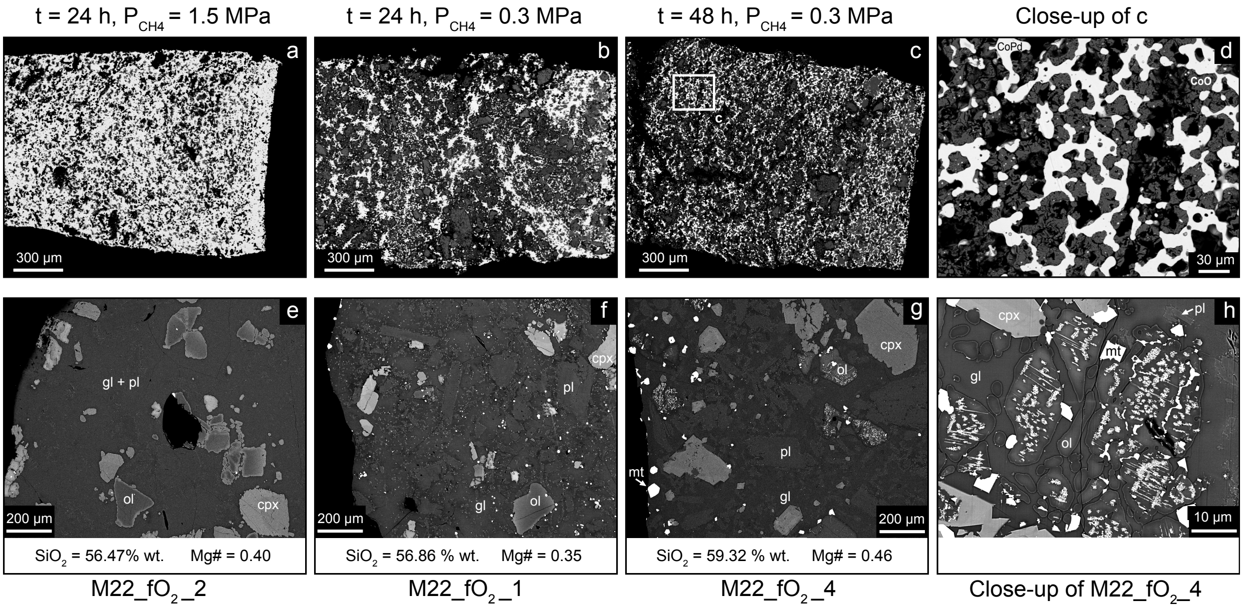

FIGURE 2. BSE images of selected oxidation experiments. (**a** to **d**) Retrieved CoPd-CoO oxygen fugacity sensors for different initial partial pressures of methane (**a** and **b**), and different run times (**b** and **c**). (**d**) A close-up of **c** shows the interconnected blebs of CoPd alloy (white) surrounded by patches of CoO (gray porous grains). (**e** to **f**) Images of experimental glasses retrieved with the sensors. (**e**) At P_{CH4} = 1.5 MPa, the charge contains zoned olivine and clinopyroxene phenocrysts, with plagioclase being hardly distinguishable from the glass. (**f**) At lower P_{CH4} = 0.3 MPa, the run experiences higher f_{O2}, which permits stabilization of tiny oxides in the groundmass. Image (**g**) and a close-up (**h**) show a run at similar P_{CH4} after 48 h, in which olivine has started to destabilize into magnetite and SiO_2 (melt). Note the crystallographic orientation of destabilization lamellae of magnetite along the olivine structure.

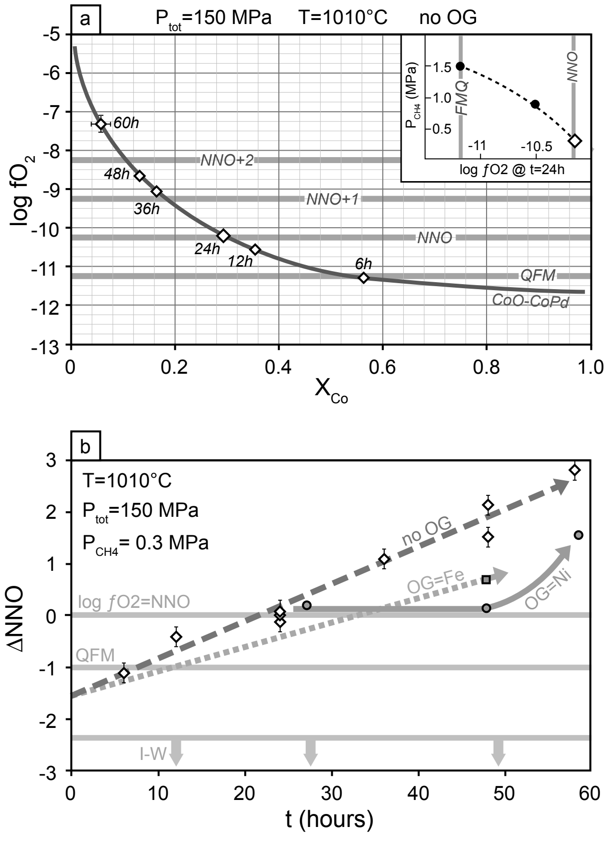

ing both EDS and WDS displayed similar values (Table 2), thus EDS was used to perform rapid and accurate quantification for the rest of the sensors. The experiments performed with no extra water within the sensor capsule (i.e., only the ambient humidity, e.g., MAS_fO2_4) and the run carried out with added H_2O (MAS_fO2_18) showed no significant difference in calculated f_{O2} (Table 2).

Effects of varying P_{CH4}

Three different values of P_{CH4} were tested (0.3, 0.9, and 1.5 MPa) corresponding to 0.2, 0.6, and 1% of the total pressure exerted on the charges. After 24 h, sensor compositions were X_{Co} = 0.3, 0.35, and 0.55, respectively, corresponding to f_{O2} values between the FMQ and NNO buffers (Fig. 3a; Table 2). Hence, as expected, higher initial P_{CH4} result in lower initial f_{O2}. We chose the more oxidized alternative for the time-series experiments (using P_{CH4} = 0.3 MPa) to examine oxygen fugacity evolution with time.

◀**FIGURE 3.** (**a**) f_{O2} variations for experiments of various durations as monitored by X_{Co}, the cobalt fraction of the CoPd alloy. The thick gray curve for the CoO-CoPd system is obtained through the equation defined in the main text. Through measurements of X_{Co}, the oxygen fugacity conditions can be calculated. The inset illustrates how f_{O2} calculated after a 24 h run can be modulated by varying the amount of CH_4 initially injected along with Ar to pressurize the vessel. (**b**) f_{O2} variations against experimental duration for charges containing no oxygen getter (labeled "no OG") and charges containing Ni and Fe as OG. For runs of up to 48 h, the range in f_{O2} traversed by the experiments can be nearly halved by inserting a Ni OG within the experimental capsule.

Time series

Experiments were quenched at *t* = 6, 12, 24, 36, 48, and 60 h to track the departure of the samples from a hypothetical chemical equilibrium, and monitor changing ambient f_{O_2} inside the charge using CoPd f_{O_2} sensors. No oxygen getters were employed in this series.

Oxygen fugacity. After 6 h, the experiments reach the FMQ buffer, at *t* = 24 h they have reached NNO, and after 60 h, the f_{O_2} conditions are around NNO+3 (Figs. 3a and 3b). The actual rates of oxidation appear to behave in a log-linear fashion, with values around 1 log unit/12 h (Fig. 3b). These oxidation rates are much faster than we had hoped, which prompted us to test whether adding oxygen getters to our charges would stabilize f_{O_2} (see below).

Phase abundances. Measured abundances show an increase in overall crystal content and a decrease in glass content (Fig. 4; Table 2). Newly formed plagioclase is the dominant crystallizing phase with an increase from ~9 vol% at *t* = 6 h to ~25 vol% at *t* = 24 h. The plagioclase content stays close to the latter value from *t* = 36 h to *t* = 60 h. Olivine shows a similar trend, increasing within runs up to *t* = 24 h and then remaining constant around 3.5 vol% until *t* = 48 h. Olivine then nearly disappears after 60 h of run time. In contrast, clinopyroxene shows a more complex behavior, with two slight increases separated by a decrease in abundance. Finally, Fe-oxides (titanomagnetite) appears in runs >12 h and slowly increases in abundance from ~0.8 to 2.4 vol% after 60 h. With respect to olivine and plagioclase mode, the data suggest that steady-state crystallinities are approached after about ~20 h.

Olivine destabilization. In the original lava sample used as initial material as well as in time-series runs quenched at *t* = 6 h and 12 h, olivine phenocrysts appear as very faintly zoned 0.1–0.3 mm crystals. In contrast, olivine in runs exceeding 24 h displays reaction textures; in BSE images, crystals appear darker and contain planar Fe-oxide lamellae (Figs. 2g and 2h). Such textures have been described in natural samples (e.g., Stromboli basalts; Cortes et al. 2006) and can develop as a consequence of oxidation. As the valence of Fe changes from 2+ to 3+, olivine rejects iron from its structure, saturating a separate Fe-oxide phase on crystallographically controlled lattice planes (e.g., Blondes et al. 2012). This impoverishment of Fe^{2+} in olivine is also evidenced by the reduced grayscale intensity of olivines within BSE images. Eventually, after 60 h, olivine almost disappears entirely from the charge.

Glass chemistry. Time-series experimental glasses show fairly complex chemical evolutions (Fig. 5; Table 3). Two processes are competing to modify the chemical composition of glasses in the time series. First and foremost, the mineral compositions and abundances need time to approach equilibrium (primarily through melting and dissolution) at the applied P_{total} and *T* conditions. Second, the progressive increase in f_{O_2} acts to shift the equilibrium, stabilizing magnetite and destabilizing olivine. Because environmental conditions progressively evolve, the equilibrium state toward which the system evolves is a moving target in these experiments.

During the first 12 h, glass SiO_2 increases while MgO and CaO decrease, and FeO remains constant (Fig. 5). This is consistent with crystallization of plagioclase, and to a lesser extent olivine and clinopyroxene. In longer experiments (*t* ≥ 24 h), as the NNO redox conditions are exceeded, compositions shift toward SiO_2 enrichment, and FeO, MgO, and CaO depletion. Since plagioclase and olivine have mostly stopped growing by *t* = 24 h (Fig. 4), these variations must be associated with crystallization of magnetite, and the moderate changes in clinopyroxene abundance. Crystallization of magnetite depletes the melt in FeO, strongly enriches the melt in SiO_2, and only has a minor effect on other elements (Fig. 5). The additional crystallization of clinopyroxene reduces CaO, MgO, and FeO. In turn, the destabilization of olivine after ~24 h is expected to slightly enrich the melt in SiO_2, MgO, and FeO, even though newly formed magnetite lamellae probably incorporate substantial Fe released from the olivines. Hence, overall, changes in glass compositions are first dominated by the tendency of the magma to chemically accommodate new pressure-temperature conditions (i.e., from initial glass-poor, crystalline crushed material to crystal-rich melt), and then affected by an upward drift in relative f_{O_2}.

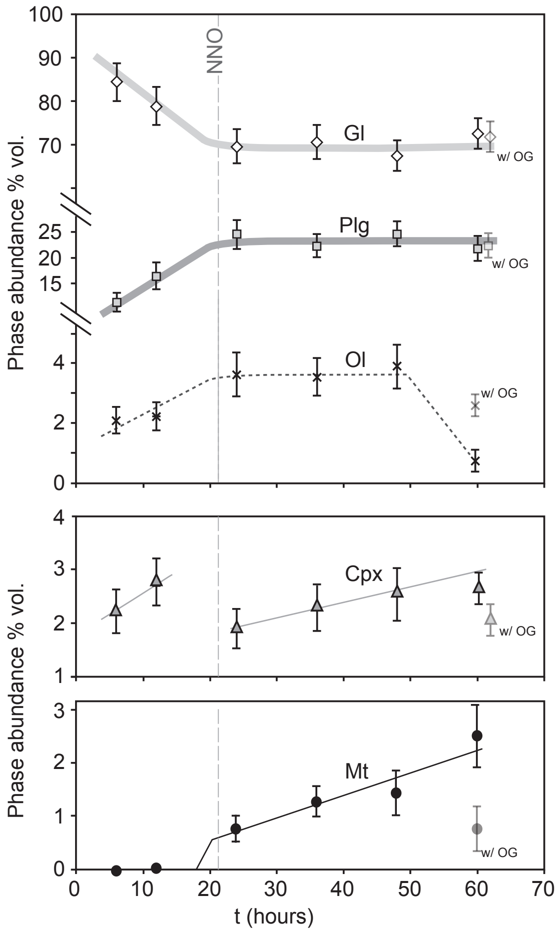

FIGURE 4. Phase abundances measured from BSE images for time-series experiments.

Effect of OGs

In view of the fast oxidation occurring within the experimental charges and the consequences for glass chemistry evolution, Fe and Ni were both tested as oxygen getters to stabilize f_{O_2}. The

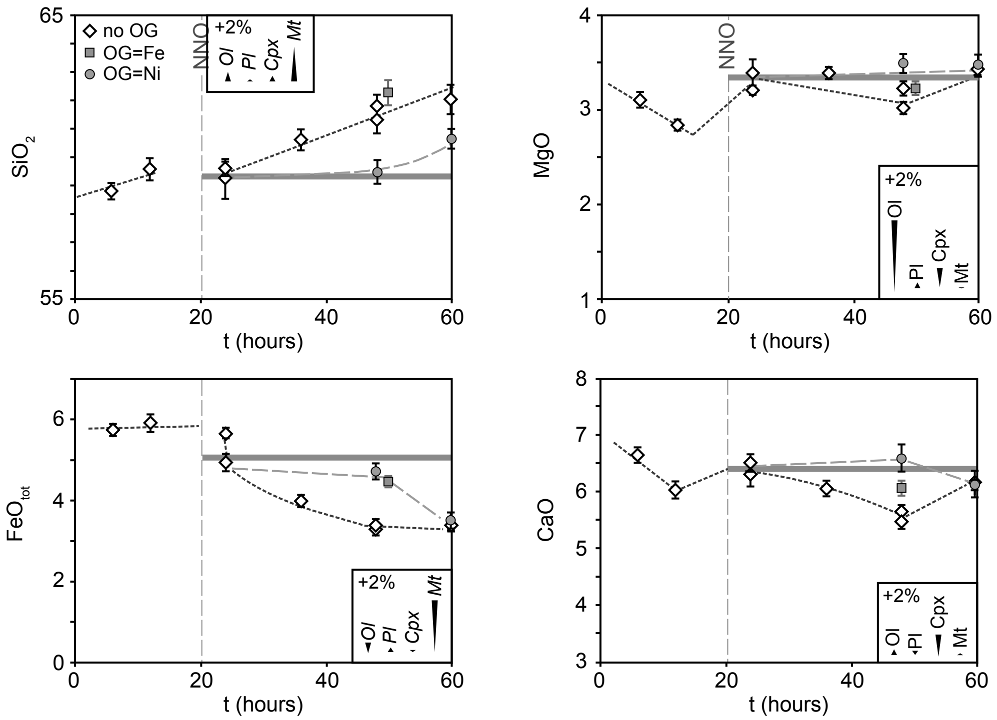

FIGURE 5. Major element glass chemistry plots for SiO_2, FeO, CaO, and MgO. Thick gray horizontal lines represent the average glass composition at $t = 24$ h. Triangles in the lower right insets show the magnitude of compositional change for addition of 2 vol% of a given phase.

TABLE 3. Major element chemistry of experimental glasses

Experiment	t (h)	SiO_2	TiO_2	Al_2O_3	FeO_{tot}	MnO	MgO	CaO	Na_2O	K_2O	P_2O_5	Totals
Variable: P_{CH4}												
MAS_fO2_1	24	56.86(0.84)	0.83(0.04)	18.21(0.21)	5.56(0.06)	0.10(0.01)	3.04(0.04)	6.43(0.10)	4.06(0.09)	1.49(0.03)	0.24(0.02)	96.82
MAS_fO2_1b	24	57.23(0.16)	0.86(0.05)	17.78(0.21)	4.78(0.19)	0.11(0.02)	3.30(0.14)	6.16(0.19)	3.99(0.08)	1.49(0.04)	0.30(0.06)	95.99
MAS_fO2_2	24	56.47(0.34)	0.80(0.01)	18.21(0.11)	5.35(0.11)	0.10(0.02)	3.56(0.08)	7.12(0.06)	4.07(0.07)	1.33(0.03)	0.25(0.01)	97.32
MAS_fO2_3	24	57.36(0.14)	0.88(0.02)	17.64(0.22)	5.65(0.11)	0.11(0.01)	3.24(0.15)	6.03(0.25)	4.08(0.09)	1.44(0.05)	0.27(0.03)	96.70
Variable: time												
MAS_fO2_4	48	59.32(0.27)	0.85(0.04)	18.14(0.17)	3.37(0.04)	0.09(0.01)	2.91(0.05)	5.24(0.05)	4.58(0.11)	1.73(0.04)	0.32(0.03)	96.54
MAS_fO2_5	12	57.63(0.37)	0.91(0.02)	17.71(0.08)	5.63(0.14)	0.11(0.01)	2.75(0.04)	5.85(0.09)	4.24(0.09)	1.59(0.06)	0.29(0.03)	96.72
MAS_fO2_6	36	58.19(0.34)	0.89(0.03)	17.76(0.10)	3.89(0.12)	0.09(0.01)	3.25(0.04)	5.84(0.08)	4.25(0.08)	1.55(0.02)	0.28(0.04)	96.01
MAS_fO2_7	6	57.17(0.23)	0.88(0.03)	18.03(0.11)	5.60(0.09)	0.11(0.02)	3.02(0.06)	6.47(0.09)	4.11(0.08)	1.54(0.05)	0.30(0.06)	97.23
MAS_fO2_8	48	58.77(0.42)	0.84(0.05)	17.80(0.12)	3.34(0.10)	0.09(0.01)	3.11(0.07)	5.40(0.10)	4.22(0.10)	1.58(0.02)	0.29(0.02)	95.46
MAS_fO2_16	60	60.61(0.24)	0.75(0.04)	18.01(0.13)	3.34(0.04)	0.08(0.01)	3.31(0.04)	5.98(0.05)	4.01(0.38)	1.39(0.02)	0.25(0.03)	97.80
Variable: OG												
MAS_fO2_13	48	57.73(0.29)	0.77(0.04)	18.14(0.16)	4.32(0.16)	0.09(0.01)	3.43(0.06)	6.47(0.16)	4.10(0.08)	1.39(0.08)	0.24(0.02)	96.69
MAS_fO2_15	60	58.30(0.37)	0.79(0.04)	16.32(0.15)	3.32(0.13)	0.08(0.01)	3.34(0.19)	5.80(0.21)	4.07(0.11)	1.39(0.09)	0.25(0.03)	95.76

major difference is that as soon as the experiments are started the Fe captures O, whereas Ni begins to seize O only after the NNO buffer curve has been met, ~20–24 h into the experiment. Thus, for a similar initial amount of OG, Fe will be exhausted earlier than Ni and will not maintain f_{O_2} stable for the same duration. After 48 h, the sensors record f_{O_2} values corresponding to NNO+0.7 (OG = Fe) and NNO+0.07 (OG = Ni), compared to ~NNO+2 without an OG (Fig. 3b). Hence, if our purpose is to maintain f_{O_2} at relatively oxidizing conditions (around NNO), Ni will be better suited than Fe because the total range of f_{O_2} crossed by the charges is more restricted. In addition, Ni has the advantage of producing a reaction product (NiO) with a characteristic green color, which makes it easy to establish whether the OG worked properly or not. The color can also be used to determine how much Ni is left unoxidized and thus to establish the potential for maintaining f_{O_2} stable in even longer subsequent experiments. To this end, two 60 h runs were performed using different amounts of Ni in the OG. In both cases, the sensors record values around NNO+1.5, implying that OGs become less efficient in maintaining f_{O_2} at t >48 h. The use of Ni as an OG maintains constant phase abundances, except for olivine which appears to decrease at t >48 h in experiments with and without OG (Fig. 4). The presence of OGs also improves the range in glass composition traversed, reducing the increase in SiO_2, and the decrease in FeO attributed to the prolonged crystallization of magnetite (Fig. 5).

Effect of replenishment

Different strategies were employed to establish whether injecting more CH_4 into the pressure line would help mitigate fast oxidation; the 48 h experiment MAS_FO2 _8 performed with a 0.3 MPa CH_4 (+Ar) hot gas-swap at $t = 24$ h shows the same f_{O_2} conditions than a normal 48 h experiment with no gas replenishment (ΔNNO ~ +1.5 to 2). A similar experiment involving a replenishment step using more methane ($P_{CH_4} = 5$ MPa, MAS_FO2_17) showed an improvement compared to the other 48 h runs (i.e., ΔNNO = +0.7). The other strategy consisted in performing cold-swaps every 24 h prior to replenishment with pressurizing gases. The resulting 72 h experiment (MAS_FO2 _9) experienced a significantly more reduced environment (ΔNNO = –1). Overall, these various sets of experiments show that while replenishment techniques can maintain f_{O_2} around NNO at durations of 72 h, more absolute variability is to be expected.

DISCUSSION

These results have important consequences for experimental investigations of hydrous mafic systems at high temperature. The consequences of not maintaining stable f_{O_2} are considered, along with implication for achieving thermodynamic equilibrium in CSPV experiments. An important preamble to this discussion is that our experimental results involve a specific composition at fixed *P*-*T* conditions, carried out within a specific laboratory setup. Considering that the type of CSPV (i.e., TZM or MHC), sheath and furnace setups, line volumes and materials employed may vary, we stress that oxygen fugacity may evolve at a different rate in different apparatus. Hence, investigators should be cautious about extrapolating our f_{O_2} conditions directly.

The challenges of maintaining stable oxygen fugacity

Experiments performed in CSPV show that oxygen fugacity conditions are not constant during runs. While the quantity of CH_4 added to the initial pressure system shifts the experimental f_{O_2} to higher or lower values (Fig. 2a), it does not affect the rate at which oxidation occurs. Instead, our time-series reveals that f_{O_2} increases by 3–4 orders of magnitude in just 48 h. This is particularly problematic for experimental runs that require equilibration times longer than just a few hours (e.g., Berndt et al. 2005). The use of OG such as Ni to capture O and counterbalance the diffusion of H_2 outside the capsule helps stabilize and maintain f_{O_2} to relatively constant values. In our runs, all OG capsules still contained unoxidized Ni powder (<1/2 the initial amount, 0.06 g), suggesting that f_{O_2} can be maintained for longer than 48 h, but not realistically for much longer. A 60 h experiment (MAS_fO2_15; Table 2) shows that even with more Ni added to the initial setup, f_{O_2} is ~1.5 log units above the desired NNO buffer value. Potentially, after a certain time, the limiting factor is not the abundance of oxygen that can be captured by the OG, but rather the depletion of hydrogen in the capsule and vessel. For experiments of up to 72 h, the runs can undergo hot- or cold-swapping, with CH_4 being re-injected every 24 h. This proved to be the only means of stabilizing f_{O_2} around NNO for over 48 h (Table 2).

Consequences of fast oxidation

Rapid changes in redox conditions affect the valence state of elements, particularly Fe in magmas, and modify minerals and the host-melt in various ways.

Stabilization of Fe-oxides. One of the major consequences of increasing f_{O_2} in melts is the crystallization of oxide phases such as magnetite (Fe_3O_4) that readily acquire the available Fe^{3+} (e.g., Osborn 1959; Toplis and Carroll 1995). This phenomenon was observed in our time-series, after about ~20 h when f_{O_2} attains NNO, and led to an increase in melt SiO_2 (from ~57 to ~59.5 wt%; Fig. 5) accompanied by a decrease in FeO (from 6 to about 3.5 wt%). Over-production of magnetite, essentially due to an experimental artifact, can cause unwanted and profound deviations from natural crystallization sequences. For example, Fe-depletion from the melt at high f_{O_2} could cause the melt to shift from a tholeiitic to a calc-alkaline magma differentiation trend (e.g., Berndt et al. 2005; Hammer 2006). Second, because Fe-bearing oxides and clinopyroxenes crystallize epitaxially (Hammer et al. 2010), the presence of magnetite could stabilize clinopyroxene earlier during the melt's evolution than would otherwise occur.

Destabilization of olivine. Mafic minerals such as olivine (and orthopyroxene) preferentially incorporate Fe^{2+} over Fe^{3+} into their structure (e.g., Nakamura and Schmalzried 1983). Hence, as f_{O_2} increases and the valence of Fe changes, olivine releases Fe, which then forms exsolution lamellae of magnetite according to the reaction

$$3Fe_2SiO_4^{Ol} + O_2 \rightarrow 2Fe_3O_4^{Mt} + 3SiO_2^{Liq}.$$

As a result, olivines destabilize and the residual olivines evolve toward more forsteritic compositions (e.g., Muan 1958; Osborn 1959; Cortes et al. 2006; Blondes et al. 2012 and references therein) (see Fig. 2). The dissolution of olivine along crystallographic planes and the ensuing percolation of melt outward into the matrix automatically cause olivine cores initially far from the melt to be in contact and possibly re-equilibrate. This effect can have deleterious effects in circumstances where Mg/Fe partition coefficients $K_{\mathrm{D\,Ol}}^{\mathrm{Fe}}/{}^{\mathrm{Mg}}_{\mathrm{Liq}}$ compositions are used to establish equilibrium. The compositional effect on the surrounding melt in our series is expected to be fairly minimal at first, since oxides incorporate the Fe released from destabilizing olivines (t = 24–48 h), and then more pronounced as entire crystals dissolve ($t > 48$ h, Fig. 4); this decrease in olivine abundance after 48 h is accompanied by slight increases in melt MgO (Fig. 5). In contrast, the distribution coefficient D_{SiO_2} between olivine and melt is close enough to unity that it is difficult for small changes in olivine abundance to greatly change the melt's SiO_2 concentration.

Effects on other phases. In contrast with olivine, plagioclase preferably includes Fe^{3+} and can be used as a geobarometer (e.g., Sugarawa 2001). Although plagioclase is the dominant mineral in the present experiments (~25 vol%; Fig. 4), it only admits up to 0.75–0.90% FeO (cf. Moore and Carmichael 1998 for plagioclase analysis). Thus, the uptake of Fe^{3+} by plagioclase should not affect the melt composition markedly. However, clinopyroxene readily incorporates both Fe^{2+} and Fe^{3+}, a property employed in geobarometry (Luth and Canil 1993; McCanta et al. 2004). Matrix glass compositions of the time-series experiments indicate that pyroxene continues to form even after most other phase abundances have stabilized (Fig. 4). This has a non-negligible effect on melt composition, primarily a decrease in MgO and CaO (Fig. 5). Since clinopyroxene is capable of incorporating larger amounts of Fe^{3+} under oxidizing conditions (McCanta et al. 2004), progressive oxidation could aid in stabilizing additional clinopyroxene (Toplis and Carroll 1995).

Assessement of progress toward chemical equilibrium

Phase equilibria, or so-called "static" experiments performed at constant *P* and *T* conditions, commonly use crushed starting material or glass previously fused at superliquidus conditions (Pichavant et al. 2007; Hammer 2008 and references therein). In the first case, equilibrium is approached dominantly by melting/dissolution, and in the second, by crystallization. In both cases, it is expected that phases will either dissolve or crystallize until a partial thermodynamic equilibrium is approached (e.g., Edgar 1973). One or more lines of evidence may be employed to demonstrate that the run time was sufficient for the system to closely approach equilibrium (Fyfe 1960; Edgar 1973; Grove and Bence 1979; Sisson and Grove 1993; Pichavant et al. 2007; Hammer 2008).

- Comparisons with experimental timescales of previous investigations that used similar compositions of reactive magma (e.g., Di Carlo et al. 2006; Feig et al. 2010).
- Idiomorphic crystal morphologies are assumed to show that phases were crystallizing and not in the process of dissolving (e.g., Toplis and Carroll 1995; Moore and Carmichael 1998; Di Carlo et al. 2006; Feig et al. 2010).
- Chemical homogeneity of crystal and glass phases of the reactive magma (e.g., Toplis and Carroll 1995; Moore and Carmichael 1998; Berndt et al. 2005; Di Carlo et al. 2006; Feig et al. 2010).
- Time independence of phase compositions (e.g., Métrich and Rutherford 1998; Gaillard et al. 2002; Berndt et al. 2005).
- Time independence of type and abundance of phases (though the crystal numbers and sizes can change through textural maturation) (e.g., Berndt et al. 2005).
- Similar phase abundances and composition in runs performed from both the crystallization and melting/dissolution sides (i.e., reversals) (e.g., Toplis and Carroll 1995; Moore et al. 1995; Hammer et al. 2002; Berndt et al. 2005).
- Equilibrium value of exchange coefficients for specific elements in the melt and minerals (i.e., partition of Fe, Mg in olivine and melt) (e.g., Grove and Bence 1979; Toplis 2005; Di Carlo et al. 2006).

Our experiments utilized natural, holocrystalline lava, to approach an equilibrium state that includes a melt phase. Thus, in terms of phase mode, it could be inferred that equilibrium was approached primarily by solid dissolution. However, crystal abundances in the shortest run were minima, with mineral abundances reaching plateaus after 20–24 h (Fig. 4). Furthermore, idiomorphic crystal shapes suggest that crystals were growing and not dissolving. Most likely, processes of coarsening and ripening (e.g., Park and Hanson 1999; Cabane et al. 2005) are responsible for the presence of faceted morphologies in most phases, and satisfactorily explain an approach to equilibrium by crystallization in our experiments.

Out of the indicators of equilibrium listed above, those that demonstrate time independence of phase abundances and chemistry are probably the most robust (Fyfe 1960; Edgar 1973 and references therein). Phase abundances are, however, most often estimated using mass balance calculations (e.g., Albarede and Provost 1977), and seldom assessed independently from glass or crystal compositions. For our runs, phase proportions were measured using 2D BSE images separately from compositions. Our independent assessments suggest that while time-invariance is a valid assessment of phase abundances after ~20–24 h (glass, plagioclase, and olivine, Fig. 4), glass compositions (Fig. 5) vary throughout the entire experimental timescale. As described above, oxidation is the likely culprit for both changing glass compositions and phase abundances (particularly magnetite, olivine, and clinopyroxene). We conclude that chemical equilibrium would be impossible to demonstrate from the compositions of phases in CSPV experiments in which oxidation proceeds at the high rates we observe. Furthermore, the near complete dissolution of olivine after 60 h violates the premise that phenocryst interiors do not form part of the reactive magma; while the effects of olivine destabilization on the melt composition are rather moderate in our series, the same cannot be expected of experiments that may have higher olivine abundances to begin with. Fortunately, these effects can be mitigated by inclusion of the Ni-OG in an experimental charge, stabilizing the glass composition for 24–48 h (Fig. 5). For runs requiring longer equilibration timescales (e.g., more felsic and/or colder magmas), charges need to be hot- or cold-swapped every ~24–48 h to maintain the magma near chemical equilibrium.

Applicable experimental durations and solutions for longer experiments

Since the rates of oxygen fugacity increase with time depends strongly on temperature (e.g., Hewitt 1978), we can expect that f_{O_2} in hotter experiments (i.e., $T > 1010$ °C) will be difficult to keep constant for more than 2 days (whereas cooler experiments can be kept at fixed conditions for longer durations). Hence, realistically, static phase equilibria runs at high *T* can be performed up to durations of about 96 h (counting one step of quenching-replenishment), whereas dynamic experiments involving decompression or cooling may be limited to a maximum of 48 h (considering that quench-replenishment steps may interfere with the changing *P* or *T* conditions). Fortunately, because the rates of chemical diffusion in the melt phase are fast within hotter mafic magmas (e.g., Watson 1994), timescales of 48–96 h are sufficient for a wide range of applications to simulate natural systems. In fact, most static and dynamic experiments involving mafic compositions are typically performed within timescales <96 h (cf. Table 1 and references therein), because these durations are deemed sufficient for such systems to reach steady-states. In natural systems involving mafic magmas, the rates of magmatic ascent are thought to be fast during both effusive and explosive eruptions (0.03–30 m/s, Klein et al. 1987; Rutherford 2008). For instance, assuming a lithostatic pressure gradient with a wallrock density $\rho = 2500$ kg/m^3, a total decompression of 100 MPa from the storage to the fragmentation level (or the free magma surface for effusive eruptions) within an experimental timeframe of 48 h allows for ascent rates as low as ~0.024 m/s. Similarly, for a total cooling of 100–150 °C, cooling rates as low as 2–3 °C/h can be applied. Therefore, overall, total durations of 48–96 h are adequate to simulate a large range of natural magmatic processes typical of mafic systems.

Nonetheless, there are cases where investigators will need to perform much longer experiments to characterize slower processes (e.g., experiments initiated near a phase boundary where transformation rates are slow, crystal ripening experiments, etc.) In such cases, alternative setups allowing experimentalists to perform runs without the burdensome steps of quenching and repressurization should be considered. The only suitable method to impose and maintain f_{O_2} in long-duration experiments involving hot mafic magmas is the Shaw-membrane technique. While it requires modifications to the CSPV setup and additional safety precautions associated with H_2, gas, it potentially allows f_{O_2} to be maintained fixed throughout an experiment for durations longer than 48 h (Scaillet et al. 1992).

ACKNOWLEDGMENTS

The authors acknowledge the NSF Grant EAR-0948728. This work benefited from the inputs of Malcolm Rutherford, Jessica Larsen, and James Gardner. Eric Hellebrand is thanked for his help setting up the EMPA analyses. Thorough reviews from the editor and from Roman Botcharnikov were appreciated and enriched this contribution significantly. Steve Parman and an anonymous reviewer are also thanked for improvements made to a previous version of the manuscript.

REFERENCES CITED

Albarède, F. and Provost A. (1977) Petrological and geochimical mass-balance equations: an algorithm for least-square fitting and general error analysis. Computers Geoscience, 3, 309–326.

Barclay, J. and Carmichael, I.S.E. (2004) A hornblende basalt from Western Mexico: Water-saturated phase relations constrain a pressure-temperature window of eruptibility. Journal of Petrology, 45, 485–506.

Barr, J.A. and Grove, T.L. (2010) AuPdFe ternary solution model and applicatiosn to understanding the f_{O_2} of hydrous, high-pressure experiments. Contributions to Mineralogy and Petrology, 160, 631–643.

Barr, J.A., Grove, T.L., and Wilson, A.H. (2009) Hydrous komatiites from Commondale, South Africa: an experimental study. Earth and Planetary Science Letters, 284, 199–207.

Berndt, J., Koepke, J., and Holtz, F. (2005) An experimental investigation of the influence of water and oxygen fugacity on differentiation of MORB at 200 MPa. Journal of Petrology, 46, 135–167.

Blondes, M.S., Brandon, M.T., Reiners, P.W., Zeb Page, F., and Kita, N.T. (2012) Generation of forsteritic olivine ($Fo_{99.8}$) by subsolidus oxidation in basaltic flows. Journal of Petrology, 53, 971–984.

Blundy, J. and Cashman, K.V. (2008) Petrologic reconstruction of magmatic system variables and processes. In K.D. Putirka and F.J. Tepley III, Eds., Minerals, Inclusions and Volcanic Processes, 69, p. 179–239. Reviews in Mineralogy and Geochemistry, Mineralogical Society of America, Chantilly, Virginia.

Boettcher, A.L. and Kerrick, D.M. (1971) Temperature calibration in cold-seal pressure vessels. In G.C. Ulmer, Ed., Research Techniques for High Pressure and High Temperature, p. 174–181. Springer-Verlag, New York.

Cabane, H., Laporte, D., and Provost, A. (2005) An experimental study of Ostwald ripening of olivine and plagioclase in silicate melts: Implications for the growth and size of crystals in magmas. Contributions to Mineralogy and Petrology, 150, 37–53.

Carmichael, I.S.E. (1991) The redox state of basic and silicic magmas: A reflection of their source regions? Contributions to Mineralogy and Petrology, 106, 129–141.

Carmichael, I.S.E. and Ghiorso, M.S. (1990) The effect of oxygen fugacity on the redox state of natural liquids and their crystallizing phases. In J. Nicholls and J.K. Russell, Eds., Modern Methods of Igneous Petrology: Understanding magmatic processes, 24, p. 191–212. Reviews in Mineralogy and Geochemistry, Mineralogical Society of America, Chantilly, Virginia.

Carmichael, I.S.E. and Nicholls, J. (1967) Iron-titanium oxides and oxygen fugacities in volcanic rocks. Journal of Geophysical Research, 72, 4665–4687. doi:10.1029/JZ072i018p04665.

Coombs, M.L., Eichelberger, J.E., and Rutherford, M.J. (2000) Magma mixing and storage conditions for the 1953–1974 eruptions of Southwest Trident volcano, Katmai National Park, Alaska. Contributions to Mineralogy and Petrology, 140, 99–118.

Cortes, J.A., Wilson, M., Condliffe, E., and Francalanci, L. (2006) The occurrence of forsterite and highly oxidizing conditions in basaltic lavas from Stromboli volcano, Italy. Journal of Petrology, 47, 1345–1373.

Dann, J.C., Holzheid, A.H., Grove, T.L., and McSween, H.Y. (2001) Phase equilibria of the Shergotty meteorite: constraints on pre-eruptive water contents of martian magmas and fractional crystallization under hydrous conditions. Meteoritics Planetary Science, 36, 793–806.

Di Carlo, I., Pichavant, M., Rotolo, S.G., and Scaillet, B. (2006) Experimental crystallization of a high-K arc basalt: The golden pumice, Stromboli volcano (Italy). Journal of Petrology, 47, 1317–1343.

Di Traglia, F., Cimarelli, C., de Rita, D., and Gimeno Torrente, D. (2009) Changing eruptive styles in basaltic explosive volcanism: examples from Croscat complex scoria cone, Garrotxa Volcanic Field (NE Iberian Peninsula). Journal of Volcanology and Geothermal Research, 180, 89–109.

Edgar, A.D. (1973) Experimental Petrology—Basic principles and techniques. Oxford University Press, New York.

Eugster, H.P. (1957) Heterogeneous reactions involving oxidation and reduction at high pressures and temperatures. Journal of Chemistry and Physics, 26, 1760–1761.

Feig, S.T., Koepke, J., and Snow, J.E. (2010) Effect of oxygen fugacity and water on phase equilibria of a hydrous tholeiitic basalt. Contributions to Mineralogy and Petrology, 160, 551–568.

Frantz, J.D. and Eugster, H.P. (1973) Acid-base buffers: use of Ag+AgCl in the experimental control of solution equilibria at elevated pressure and temperatures. American Journal of Science, 273, 269–296.

Fyfe, W.S. (1960) Hydrothermal synthesis and determination of equilibrium between minerals in the subliquidus region. Journal of Geology, 68, 553–566.

Gaetani, G.A. and Grove, T.L. (1998) The influence of water on melting of peridotite. Contributions to Mineralogy and Petrology, 131, 323–346.

Gaetani, G.A., Grove, T.L., and Bryan, W.B. (1994) Experimental phase relations of basaltic andesite from hole 839B under hydrous and anhydrous conditions. Proceedings of the Ocean Drilling Program: Scientific Results, 135, 557–563.

Gaillard, F., Scaillet, B., and Pichavant, M. (2002) Kinetics of oxidation-reduction in hydrous silicic melts. American Mineralogist, 87, 829–837.

Gardner, J.E., Rutherford, M.J., Carey, S. and Sigurdsson, H. (1995) Experimental constraints on pre-eruptive water contents and changing magma storage prior to the explosive eruptions of Mt. St. Helens volcano. Bulletin of Volcanology, 57, 1–17.

Grove, T.L. (1981) Use of FePt alloys to eliminate the iron loss problem in 1 atmosphere gas mixing melting experiments: Theoretical and practical considerations. Contributions to Mineralogy and Petrology, 78, 298–304.

Grove, T.L. and Bence, A.E. (1979) Crystallization kinetics in a multiply saturated basalt magma, An experimental study of Luna 24 ferrobasalt. Proceedings of the 10th Lunar Science Conference, 10, 439–478.

Grove, T.L., Donnelly-Nolan, J.M., and Housh, T. (1997) Magmatic processes that generated the rhyolite of Glass Mountain, Medicine Lake Volcano, N. California. Contributions to Mineralogy and Petrology, 127, 205–223.

Gunter, W.D., Myers, J., and Girsperger, S. (1987) Hydrogen, metal membranes. In G.C. Ulmer and H.L. Barnes, Eds., Hydrothermal Experimental Techniques, p. 100–120. Wiley, New York.

Hammer, J.E. (2006) Influence of f_{O_2} and cooling rate on the kinetics and energetics of Fe-rich basalt crystallization. Earth and Planetary Science Letters, 248, 618–637, DOI: 10.1016/j.epsl.2006.04.022.

——— (2008) Experimental studies of the kinetics and energetics of magma crystallization. In K.D. Putirka and F.J. Tepley III, Eds., Minerals, inclusions and volcanic processes, 69, p. 9–59. Reviews in Mineralogy and Geochemistry, Mineralogical Society of America, Chantilly, Virginia.

Hammer, J.E., Rutherford, M.J., and Hildreth, W. (2002) Magma storage prior to the 1912 eruption at Novarupta, Alaska. Contributions to Mineralogy and Petrology, 144, 144–162.

Hammer, J.E., Sharp, T.G., and Wessel, P. (2010) Heterogeneous nucleation and epitaxial crystal growth of magmatic minerals. Geology, 38, 367–370.

Hewitt, D.A. (1978) A redetermination of the fayalite-magnetite-quartz equilibrium between 650 and 850°C. American Journal of Science, 278, 715–724.

Holloway, J.R. (1971) Internally-heated pressure vessels. In G.C. Ulmer, Ed., Research techniques for high pressure and high temperature, p. 217–258. Springer-Verlag, New York.

Holloway, J.R. and Wood, B.J. (1988) Simulating the Earth: Experimental geochemistry. Unwin Hyman, Massachusetts.

Houghton, B.F. and Gonnerman, H.M. (2008) Basaltic explosive volcanism: Constraints from deposits and models. Chemie der Erde, 2, 117–140.

Huebner, J.S. (1971) Buffering techniques for hydrostatic systems at elevated pressures. In G.C. Ulmer, Ed., Research Techniques for High Pressure and High Temperature, p. 123–178. Springer-Verlag, New York.

——— (1987) Use of gas mixtures at low pressure to specify oxygen and other fugacities of furnace atmospheres. In G.C. Ulmer and H.L. Barnes, Eds., Hydrothermal Experimental Techniques, p. 20–60. Wiley, New York.

Jarosewich, E., Nelen, J.A., and Norberg, J.A. (1980) Reference samples for electron microprobe analysis. Geostandards Newsletter, 4, 43–47.

Klein, F.W., Koyanagi, R.Y., Nakata, J.S., and Tanigawa, W.R. (1987) The seismicity of Kilauea's magma system. U.S. Geological Survey Professional Paper, 1350, p. 1019–1185.

Kouchi, A. and Sunagawa, I. (1983) Mixing basaltic and dacitic magmas by forced convection. Nature, 304, 527–528.

Lange, R.A. and Carmichael, I.S.E. (1990) Hydrous basaltic andesites associated with minette and related lavas in western Mexico. Journal of Petrology, 31, 1225–1259.

Lofgren, G. (1987) Internally heated systems. In G.C. Ulmer and H.L. Barnes, Eds., Hydrothermal Experimental Techniques, p. 325–332. Wiley, New York.

Luth, R.W. and Canil, D. (1993) Ferric iron in mantle-derived pyroxenes and a new oxybarometer for the mantle. Contributions to Mineralogy and Petrology, 113, 236–248.

Matthews, W., Linnen, R.L., and Guo, Q. (2003) A filler-rod technique for controlling redox conditions in cold-seal-pressure vessels. American Mineralogist, 88, 701–707.

McCanta, M.C., Dyar, M.D., Rutherford, M.J., and Delaney, J.S. (2004) Iron partitioning between basaltic melts and clinopyroxene as a function of oxygen fugacity. American Mineralogist, 89, 1685–1693.

Métrich, N. and Rutherford, M.J. (1998) low-pressure crystallization paths of H_2O-saturated basaltic-hawaiitic melts from Mt. Etna: Implications for open-system degassing of basaltic volcanoes. Geochimica et Cosmochimica Acta, 62, 1195–1205.

Moore, G. and Carmichael, I.S.E. (1998) The hydrous phase equilibria (to 3 kbar) of an andesite and basaltic andesite from western Mexico: Constraints on water content and conditions of phenocryst growth. Contributions to Mineralogy and Petrology, 130, 304–319.

Moore, G., Righter, K., and Carmichael, I.S.E. (1995) The effect of dissolved water on the oxidation state of iron in natural silicate liquids. Contributions to Mineralogy and Petrology, 120, 170–179.

Moore, G., Vennemann, T., and Carmichael, I.S.E. (1998) An empirical model for the solubility of H_2O in magmas to 3 kilobars. American Mineralogist, 83, 36–42.

Muncill, G.E. and Lasaga, A.C. (1988) Crystal-growth kinetics of plagioclase in igneous systems: Isothermal H_2O-saturated experiments and extension of a growth model to complex silicate melts. American Mineralogist, 73, 982–992.

Muan, A. (1958) Phase equilibria at high temperature in oxide systems involving changes in oxidation states. American Journal of Science, 256, 171–207.

Mysen, B.O. (2006) Redox equilibria of iron and silicate melt structure: Implications for olivine/melt element partitioning. Geochimica et Cosmochimica Acta, 70, 3121–3138.

Nafziger, R.H. (1971) Gaseous buffering for the control of oxygen fugacity at one atmosphere. In G.C. Ulmer GC, Ed., Research Techniques for High Pressure and High Temperature, p. 9–42. Springer-Verlag, New York.

Nakamura, A. and Schmalzried, H. (1983) On the stoichiometry and point defects of olivine. Physics and Chemistry of Minerals, 23, 345–353.

O'Neill, H.St.C. and Pownceby, M.I. (1993) Thermodynamic data from redox reactions at high temperatures. I. An experimental and theoretical assessment of the electrochemical method using stabilized zirconia electrolytes, with revised values for the Fe-"FeO," Co-CoO, Ni-NiO and Cu-Cu_2O oxygen buffers, and new data for the W-WO_2 buffer. Contributions to Mineralogy and Petrology, 114, 296–314.

Osborn, E.F. (1959) Role of oxygen pressure in the crystallization and differentiation of basaltic magma. American Journal of Science, 257, 609–647.

Park, Y. and Hanson, B. (1999) Experimental investigations of Ostwald-ripening rates of forsterite in the haplobasaltic system. Journal of Volcanology and Geothermal Research, 90, 103–113.

Parman, S.W., Dann, J.C., Grove, T.L., and de Wit, M.J. (1997) Emplacement conditions of komatiite magmas from the 3.49 Ga Komati formation, Barberton greenstone belt, South Africa. Earth and Planetary Science Letters, 150, 303–323.

Pichavant, M., Martel, C., Bourdier, J.-L., and Scaillet, B. (2002) Physical conditions, structure, and dynamics of a zoned magma chamber: Mount Pelee (Martinique, Lesser Antilles arc). Journal of Geophysical Research, 107, B52093.

Pichavant, M., Costa, F., Burgisser, A., Scaillet, B., Martel, C., and Poussineau, S. (2007) Equilibration scales in silicic to intermediate magmas: Implications for experimental studies. Journal of Petrology, 48, 1955–1972.

Pownceby, M.I. and O'Neill, H.St.C. (1994) Thermodynamic data from redox reactions at high temperatures. III. Activity-composition relations in Ni-Pd alloys from EMF measurements at 850–1250 K, and calibration of the NiO + Ni-Pd assemblage as a redox sensor. Contributions to Mineralogy and Petrology, 116, 327–339.

Rutherford, M.J. (2008) Magma ascent rates. In K.D. Putirka and F.J. Tepley III, Eds., Minerals, Inclusions and Volcanic Processes, 69, p. 241–271. Reviews in Mineralogy and Geochemistry, Mineralogical Society of America, Chantilly, Virginia.

Scaillet, B., Pichavant, M., Roux, J., Humbert, G., and Lefèvre, A. (1992) Improvements of the Shaw membrane technique for measurement and control of f_{H_2} at high temperatures and pressure. American Mineralogist, 77, 647–655.

Schmidt, B., Scaillet, B., and Holtz, F. (1995) Accurate control of fH_2 in cold-seal pressure vessels with the Shaw membrane technique. European Journal of Mineralogy, 7, 893–903.

Shaw, H.R. (1963) Hydrogen-vapor mixtures; Control of hydrothermal experiments by hydrogen osmosis. Science, 139, 1220–1222.

Simakin, A.G., Salova, T.P., and Babansky, A.D. (2009) Amphibole crystallization from a water-saturated andesite melt: Experimental data at P = 2 kbar. Petrology, 17, 591–605.

Sisson, T.W. and Grove, T.L. (1993) Experimental investigations of the role of H_2O in calc-alkaline differentiation and subduction zone magmatism. Contributions to Mineralogy and Petrology, 113, 143–166.

Spulber, S. and Rutherford, M.J. (1983) The origin of rhyolite and plagiogranite in oceanic crust: an experimental study. Journal of Petrology, 24, 1–25.

Sugawara, T. (2001) Ferric iron partitioning between plagioclase and silicate liquid: Thermodynamics and petrologicaly applications. Contributions to Mineralogy and Petrology, 141, 659–686.

Taylor, J.R., Wall, V.J., and Pownceby, M.I. (1992) The calibration and application of accurate redox sensors. American Mineralogist, 77, 284–295.

Toplis, M.J. (2005) The thermodynamics of iron and magnesium partitioning between olivine and liquid: criteria for assessing and predicting equilibrium in natural and experimental systems. Contributions to Mineralogy and Petrology, 149, 22–39.

Toplis, M.J. and Carroll, M.R. (1995) An experimental study of the influence of oxygen fugacity on Fe-Ti oxide stability, phase relations, and mineral-melt equilibria in ferro-basaltic systems. Journal of Petrology, 36, 1137–1170.

Wilke, M. and Behrens, H. (1999) The dependence of the partitioning of iron and europium between plagioclase and hydrous tonalitic melt on oxygen fugacity. Contributions to Mineralogy and Petrology, 137, 102–114.

Zhang, Y. and Cherniak, D.J. (2010) Diffusion in minerals and melts: introduction. In Y. Zhang and D.J. Cherniak, Eds., Diffusion in Minerals and Melts, 72, p. 1–4. Reviews in Mineralogy and Geochemistry, Mineralogical Society of America, Chantilly, Virginia.

Manuscript received June 3, 2012
Manuscript accepted February 7, 2013
Manuscript handled by Don Baker